Photoluminescence and electronic transition behaviors of single-stranded DNA

Qiujin Wang,[1] Shuo Lin,[1] Xuan Liu,[1] Wen Xu,[2,1,3,*] Yiming Xiao ✺,[1] Changneng Liang,[1] Lan Ding ✺,[1,†] and F. M. Peeters[1,4]

[1]*School of Physics and Astronomy and Key Lab of Quantum Information of Yunnan Province, Yunnan University, Kunming 650091, China*
[2]*Micro Optical Instruments Inc., 518118 Shenzhen, China*
[3]*Key Laboratory of Material Physics, Institute of Solid State Physics, Chinese Academy of Science, Hefei 230031, China*
[4]*Department of Physics, University of Antwerp, Groenenborgerlaan 171, B-2020 Antwerpen, Belgium*

Due to the potential application of DNA for biophysics and optoelectronics, the electronic energy states and transitions of this genetic material have attracted a great deal of attention recently. However, the fluorescence and corresponding physical process of DNA under optical excitation with photon energies below ultraviolet are still not fully clear. In this work, we experimentally investigate the photoluminescence (PL) properties of single-stranded DNA (ssDNA) samples under near-ultraviolet (NUV) and visible excitations ($270 \sim 440$ nm). Based on the dependence of the PL peak wavelength (λ_{em}) upon the excitation wavelength (λ_{ex}), the PL behaviors of ssDNA can be approximately classified into two categories. In the relatively short excitation wavelength regime, λ_{em} is nearly constant due to exciton-like transitions associated with delocalized excitonic states and excimer states. In the relatively long excitation wavelength range, a linear relation of $\lambda_{em} = A\lambda_{ex} + B$ with $A > 0$ or $A < 0$ can be observed, which comes from electronic transitions related to coupled vibrational-electronic levels. Moreover, the transition channels in different excitation wavelength regimes and the effects of strand length and base type can be analyzed on the basis of these results. These important findings not only can give a general description of the electronic energy states and transitional behaviors of ssDNA samples under NUV and visible excitations, but also can be the basis for the application of DNA in nanoelectronics and optoelectronics.

I. INTRODUCTION

Since the discovery of the deoxyribonucleic acid (DNA) structure as reported by Watson and Crick in 1953 [1], this genetic material has been a center of attention for scientific research and wide areas of applications. The DNA molecule, well known for the storage and transmission of the genetic code of all living species, is usually composed of two polynucleotide strands coiled around each other to form a double helix. The monomer unit of each strand is a nucleotide containing nucleobases, deoxyribose, and phosphoric acid. Over the past decades, the study of DNA not only laid the foundation for genomics and molecular biology, but also opened up new fields of research in physics and electronics. For example, DNA has attracted many research interests in nanoelectronics recently due to its potential application in working as a template for assembling nanocircuits and as an element of such circuits [2–6].

Undoubtedly, the in-depth understanding of the electronic structure (electronic states) and electronic transition in DNA plays a significant and important role in the application of DNA for electronics and optoelectronics. Similarly to other conventional electronic and optoelectronic materials, the features of transition among different states and channels, the charge transfer under external field (e.g., electrical and optical) driving, the electrical and optical responses, etc., in DNA are the key physical properties that we are interested in. Meanwhile and particularly, it has been realized that the mechanisms of photostability and photoinduced damage of DNA are also directly related to the electronic states and transitions in DNA structures [7–9]. At present, three following facts hamper the study of DNA's electronic properties. First, DNA is neither a periodic lattice system such as a single crystal nor truly random. A recent work pointed out that it may show long-range correlations [10], which are difficult to analyze. Second, the non-negligible forces between water or other solvent molecules and DNA contribute to random electronic surroundings. Thus, it is insufficient to consider simply the DNA molecule itself. Furthermore, the strong influence of molecular vibrations can also result in extra freedom in the analysis of DNA. In short, DNA is a highly dynamic and complex system due to these structural, environmental, and vibrational features. In this research field, the concepts based on electronic transitions among electronic states in DNA, borrowed from solid-state physics and electronics, have been demonstrated to be very useful and significant for the investigation of DNA from the viewpoint of physics [11]. However, to date, this topic still remains somewhat controversial.

Optical experiments have been widely utilized to study the possible electronic energy structures and transition behaviors of DNA and its related biomolecules. These experimental methods include optical absorption spectroscopy [8,12–15], photoluminescence (PL) [13,15–18], transient pump-probe spectroscopy (PPS) [19–21], etc. For example, the absorption spectra of the nucleic acids and their various components were measured in the far-ultraviolet as early as 1963 [12].

*wenxu_issp@aliyun.com
†dinglan@ynu.edu.cn

034412-1

Before the 1990s, by applying PL and transient PPS mainly based on ultraviolet (UV) excitations, many works preliminarily investigated the electronic states, especially the excited singlet states, of nucleic acid systems, and explored the effects of temperature, pH value, and light polarization on DNA's electronic properties such as transition wavelength, lifetime, and PL quantum yield [17,22–25]. Since 2000, thanks to the progress made in optoelectronic instrumental techniques, more and more knowledge of the electronic transitions of DNA has been accumulated [9,11]. The Crespo-Hernández group demonstrated that vertical base stacking controls the dynamics of excited singlet electronic states in single- and double-stranded oligonucleotides based on transient PPS [7]. Marguet and co-workers experimentally obtained the timescales of thymine dimer formation [8]. By applying femtosecond PPS, Buchvarov and co-workers investigated the electronic energy delocalization and dissipation in single- and double-stranded DNA [26]. Based on the PL of unmodified DNA, Backman's group investigated a photoswitching process of native nucleotides and realized superresolution intrinsic fluorescence imaging of chromatin [27]. Besides these experimental researches, people also achieved important theoretical results in this field. For instance, the electronic properties of DNA, as well as the effects of structure, molecular stretching and twisting, and water and counterions were discussed based on density-functional theory [11]. Moreover, the nonlinear response function of a DNA duplex helix [28] and specific DNA conformational modes responsible for significant changes in the exciton parentage [29] were also calculated and revealed.

It is obvious that most of the experimental and theoretical works mentioned above are focused mainly on the relaxation or absorption behaviors of excited electrons, which are pumped to the excited singlet states by UV light with a wavelength of less than 270 nm. This concern for the UV excitation or pumping is mainly owing to the mechanism that DNA dissipating excess energy from absorbed solar UV light is essential to understand the vulnerability of all genetic material to photodamage and subsequent mutations [7,26]. However, up to now, detailed knowledge of the electronic transitions from the ground state in DNA, induced by near-UV (NUV) and visible light and the corresponding electronic states, is still far from sufficient, which is the prime motivation of this work.

Here, we investigate the PL properties of single-stranded DNA (ssDNA) samples excited by NUV and visible light with different wavelengths (270 ∼ 440 nm) at room temperature, and analyze the corresponding electronic states and transition behaviors of ssDNA. There are two reasons why we choose ssDNA rather than double-stranded DNA as the research object in this work: (1) ssDNA provides an ideal platform for studying the effects of base stacking on electronic states of nucleic acid in the absence of base pairing [7]; (2) it is more flexible and can more readily obtain the undertwisted conformation that promotes dimerization [9]. Meanwhile, it should be noted that the PL spectra of the ssDNA samples are measured without adding any fluorescent probe in this study. Although the fluorescent probes can enhance the PL signals and are consequently widely used in biology [30–33], these additional probes usually lead to a complex experimental pro-
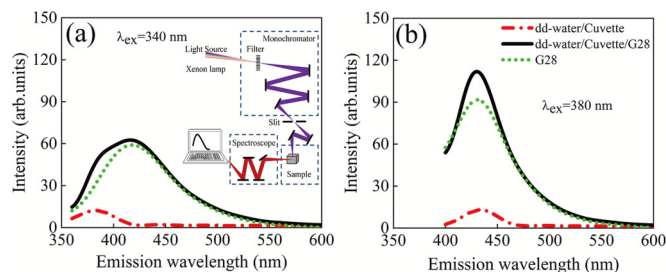
FIG. 1. PL spectra of the dd-water in a cuvette, G28 solution in a cuvette, and G28 at the excitation wavelengths of (a) 340 nm and (b) 380 nm. Note that the process of achieving the relative PL spectrum of G28 shown here is also valid for the cases of other excitation wavelengths or other samples. The inset to (a) shows the schematic diagram of the experimental setup.

cess, high cost, and to the pollution of samples. Therefore, fluorescent probes have not been used in our measurements. The ssDNA samples with sequences containing nucleobases of only one type of adenine (A), cytosine (C), thymine (T), and guanine (G) structure with different base numbers are measured by using nontransient PL and photoluminescence excitation spectroscopy, respectively. Based on the PL properties, we provide a physical description for the electronic states and transition behaviors of ssDNA samples under NUV and visible excitations. These results may find potential applications in nanoelectronics and optoelectronics based on DNA.

II. SAMPLE PREPARATION AND EXPERIMENTAL SETUP

In this work, the ssDNA samples are prepared by using solid-phase phosphoramidite triester method [34,35] with an automatic synthesizer (Bioautomation-MerMade-192E DNA/RNA). The strand sequence of each ssDNA sample contains a certain number of nucleobases of only one type of A, C, T, and G base. For a given kind of nucleobase, we prepared the samples with base numbers (N) of 28, 35, and 56. Table I shows the information for a set of samples with $N = 28$ as examples. By using double-distilled water (dd-water) as solvent, all samples are prepared as a solution form with unified ssDNA concentration of 5 μmol/L. The ssDNA solution is contained in cuvettes. The PL and PL excitation (PLE) spectra for the ssDNA samples are measured by employing a multifunctional fluorescence system (HORIBA, USA), as illustrated in the inset to Fig. 1(a). A xenon lamp with a radiation wavelength range from 240 nm to 850 nm is taken as the light source. The broadband light beam is monocolored by a monochromator (Gemini 180), which is used for tuning the excitation wavelength. Under the illumination of the excitation light, the PL emission from the sample can be detected by a grating spectrometer (iHR320) together with a photomultiplier tube (PMT). In the measurement, the excitation light beam is applied at an angle of about 45° to the sample surface, and the detection is undertaken at about 60° to the sample surface. The accuracy of the spectral measurement is 0.2 nm. Note that the experiment is performed at room temperature. At a given excitation wavelength λ_{ex}, the PL spectrum of the sample solution in a cuvette can be obtained as $I_{sr}(\lambda_e)$, in which λ_e denotes the emission wavelength (not

TABLE I. The base sequences of the ssDNA samples.

Sample No.	Base (number)	Sequence
T28	Thymine (28)	5′-TTTTTTTTTTTTTTTTTTTTTTTTTTTT-3′
A28	Adenine (28)	5′-AAAAAAAAAAAAAAAAAAAAAAAAAAAA-3′
C28	Cytosine (28)	5′-CCCCCCCCCCCCCCCCCCCCCCCCCCCC-3′
G28	Guanine (28)	5′-GGGGGGGGGGGGGGGGGGGGGGGGGGGG-3′

only emission peak wavelength). Meanwhile, the PL spectrum of the dd-water in a cuvette $I_r(\lambda_e)$ is measured as reference. To eliminate the influence of the solvent and container, the relative PL spectrum of ssDNA $I_s(\lambda_e)$ can be achieved by $I_s(\lambda_e) = I_{sr}(\lambda_e) - I_r(\lambda_e)$. In Fig. 1, we take G28 as an example for this process.

Furthermore, since the excitation photon energy and excitation power or intensity in our experiment are weak enough, the ssDNA molecules are not damaged and the observed PL spectra of all samples are stable. First, previous works usually discussed the mechanism that DNA dissipate excess energy from absorbed solar UV light, and demonstrated that DNA is intrinsically photostable under UV excitation (e.g., $\lambda_{ex} \leqslant$ 270 nm) [7,26]. Therefore, for excitation wavelengths in the NUV and visible regimes (270 ∼ 440 nm), the lower photon energy also cannot modify the ssDNA molecular structure here. In addition, we know that the PL spectra were stable for excitation intensity or power below 2 GW/cm^2 (at 266 nm) [7], 25 kW/cm^2 (at 430, 532, and 560 nm) [27], and 1 W (at 270 nm) [26]. In our work, the monocolored excitation intensities (powers) depending on the wavelength are in the range of 0.6 ∼ 1 mW/cm^2 (0.3 ∼ 0.5 mW), which is much lower than that used in previous works. Meanwhile, due to the strong absorption of the excitation light by dd-water, the light intensity experienced by ssDNA molecules can become still weaker. Accordingly, the excitation light used here cannot damage the ssDNA molecules and affect the PL stability. Moreover, the quantum yield of the fluorescence of our samples is in the range of ∼0.01% to ∼0.1% [22,27], which was also measured and used in some early works associated with nucleic acids.

III. RESULTS AND DISCUSSION

First, we measure the PL spectra of the ssDNA samples and examine mainly the dependence of the PL peak wavelength (λ_{em}) upon the pumping or excitation wavelength (λ_{ex}). For a given kind of base, we find that the spectral line shape of PL and emission peak position corresponding to each excitation wavelength are not sensitive to the base number N, whereas the fluorescence intensity increases with increasing N. Although here we only present the results of T28, T35, and T56 in Figs. 2(a) to 2(c) for simplicity, the situations of A-, C-, and G-based ssDNA samples are similar. Accordingly, in our further discussion we mainly focus on the PL properties of the samples with $N = 28$ (i.e., A28, C28, T28, and G28), whose emission spectra for $\lambda_{ex} = 270 \sim 400$ nm are provided in Fig. 2. To investigate the electronic energy states of ssDNA, we can plot the emission peak wavelength (λ_{em}) as a function of the excitation wavelength (λ_{ex}) for ssDNA with different base types (T, A, C, and G), as shown in Figs. 3(a) to 3(d).

For clarity, each λ_{em}-λ_{ex} relation can be divided into different intervals based on the variation of the curve. It is obvious that in the short excitation wavelength regime (I), λ_{em} for different samples depends very weakly on λ_{ex}, where $\lambda_{em} \approx 419$ nm for T28, 422 nm for A28, 430 nm for C28, and 406 nm for G28. These emission peak wavelengths are close to the results for UV excitation reported in previous works [24,27]. In regime I, the λ_{em}-independent emission behavior can mainly be attributed to exciton-like electronic transitions [36,37]. It is well known that excitons are quasiparticles and perceived as the solid-state counterpart of atoms. Specifically, the absorption of a photon by an interband transition in a material system creates oppositely charged particles, i.e., an electron and a hole, which can attract each other through Coulomb interaction. Under some conditions, this attractive interaction can lead to the formation of a bound electron-hole pair, which is called the exciton and can be conceived as a small hydrogenic system [38]. From the perspective of PL spectral characteristics, the emission peak wavelength associated with the exciton or exciton-like transition is nearly independent of the excitation wavelength, which is exactly the situation discussed here.

Details can be found in the energy-level diagram depicted in the left panel of Fig. 4. The energy difference between the ground and excited states (including the excimer or exciplex state and excited singlet state) for excitonic transitions differs for ssDNA with different bases, which results in diverse peak wavelengths (λ_{em}) for different samples. Furthermore, it is known that poorly stacked and well-stacked single bases usually coexist in nucleic acid samples. Thus, in regime I, the effects of base stacking on the electronic state of DNA can play an important role, which was demonstrated in previous works [7,9]. Specifically, for ssDNA with well-stacked bases, the absorption of excitation light, i.e., UV and NUV here, can transfer electrons from the electronic ground state (S_0) to the so called delocalized exciton states (S_{DE}), which are induced by the spread of the electronic wave functions over the bases in a stack [26]. Due to this kind of exciton-state delocalization, ssDNA can absorb photons with different wavelengths in a narrow band, such as $\lambda_{ex} = 300 \sim 330$ nm for A28 and T28 and $\lambda_{ex} = 270 \sim 300$ nm for C28 and G28. This narrow band can also be expressed by using an energy broadening δE_{DE}, which is the difference between the highest and the lowest energies of excitation photons. Then, the electrons in S_{DE} decay to excimer states (S_E) on an ultrafast timescale (several 100 fs) [7], followed by relaxation to S_0 with photon emission. An excimer or excited dimer is formed by neighboring aromatic molecules in their excited singlet state (S_1). At the excimer equilibrium distance, the molecules attract each other in the excited state but repel each other in the ground state. As a consequence, by comparing with the PL of base monomers
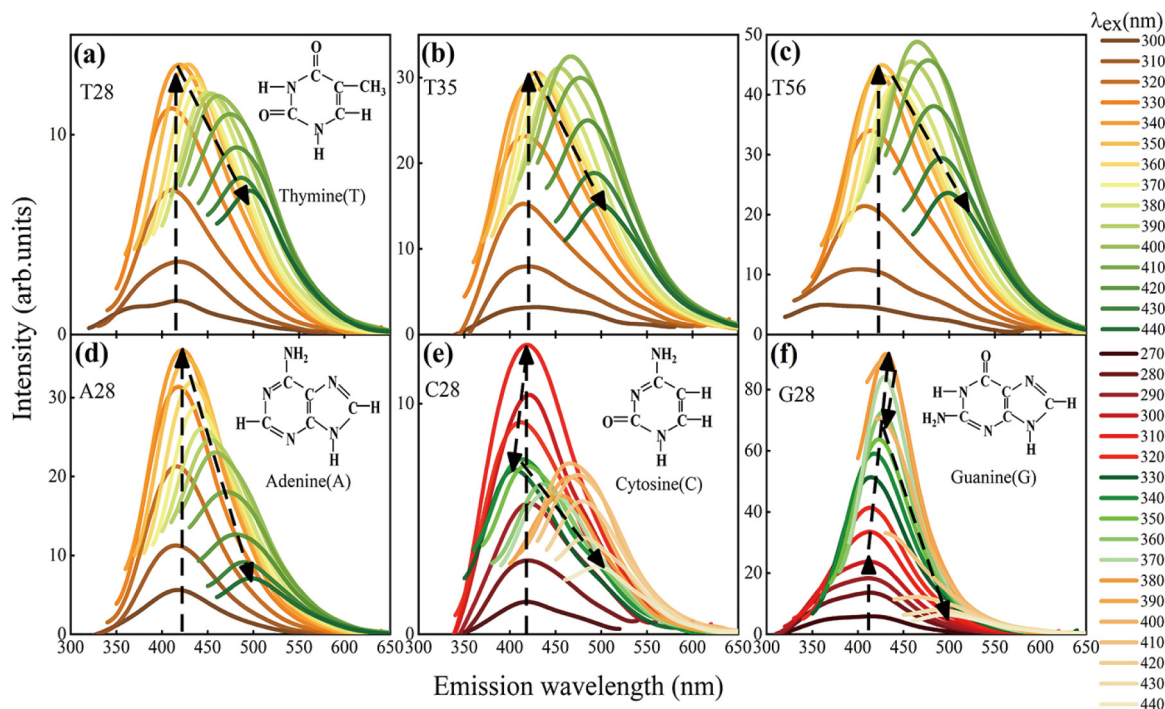
FIG. 2. PL spectra for ssDNA samples of (a) T28, (b) T35, (c) T56, (d) A28, (e) C28, and (f) G28 at different excitation wavelengths. The dashed black arrows indicate the movement trend of the peak positions and the insets show the corresponding nucleic acid structures.

excited by UV light [17,23,25], excimer fluorescence is red-shifted from them and shows no vibrational fine structure (i.e., coupled vibrational-electronic levels) [39]. Thus, the observed PL peak positions of the samples are nearly constants in regime I. Moreover, the energy parameters associated with the electronic states or transitions in this regime can be derived easily through the experimental data, which are listed in

Table II. In addition to δE_{DE}, the energy difference between the lowest level in S_{DE} and the ground state S_0 can be obtained by $\Delta E_{DE-L} \approx hc/\lambda_{ex-MAX}$, while the difference between S_E and S_0 is calculated by $\Delta E_E \approx hc/\lambda_{em}$, where h, c, and λ_{ex-MAX} are the Planck constant, the speed of light in vacuum, and the maximum of the excitation wavelength in this regime for a specific sample, respectively. Furthermore, the energy
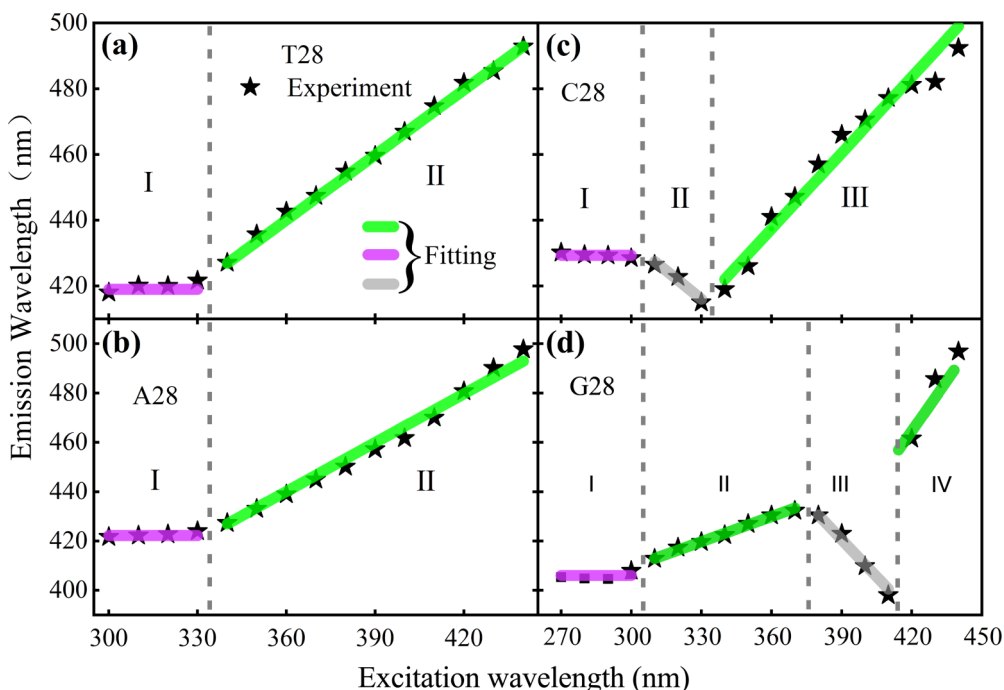
FIG. 3. The emission peak wavelength (λ_{em}) as a function of the excitation wavelength (λ_{ex}) for (a) T28, (b) A28, (c) C28, and (d) G28.

TABLE II. The energy parameters associated with the electronic states or transitions for different wavelength regimes. The asterisk (*) indicates data that correspond to $\lambda_{ex} = 400$ nm instead of $\lambda_{ex} = 410$ nm, since the measurement noise or error of the PL at $\lambda_{ex} = 410$ nm for G28 is larger and leads to $\Delta E_{shift\text{-}III}$ slightly below zero.

	I (Well-stacked base domain)			II to IV (Vibrational-electronic coupling domain)		
Sample No.	$\Delta E_{DE\text{-}L} + \delta E_{DE}$ (eV)	ΔE_E (eV)	$\Delta E_{shift\text{-}I}$ (eV)	$\Delta E_{shift\text{-}II}$ (eV)	$\Delta E_{shift\text{-}III}$ (eV)	$\Delta E_{shift\text{-}IV}$ (eV)
T28	~3.76+0.37	~2.96	~0.80	[0.30, 0.74]		
A28	~3.76+0.37	~2.94	~0.79	[0.30, 0.74]		
C28	~4.13+0.46	~2.89	~1.24	[0.77, 1.10]	[0.33, 0.71]	
G28	~4.13+0.46	~3.05	~1.08	[0.49, 1.00]	[0.08*, 0.38]	[0.27, 0.31]

shift induced by the nonradiative relaxation from the the lowest level in S_{DE} to the excimer state S_E can be obtained by $\Delta E_{shift\text{-}I} = \Delta E_{DE\text{-}L} - \Delta E_E$.

Next, at long wavelength excitations, λ_{em} of ssDNA depends strongly on λ_{ex} and different samples show different dependencies. One can see from Figs. 3(a) and 3(b) that for T28 and A28, λ_{em} increases or redshifts roughly linearly with λ_{ex}, which can be fitted by $\lambda_{em} = A\lambda_{ex} + B$, where $A = 0.66$ and $B = 202.5$ nm for both of them. Meanwhile, the λ_{em}-λ_{ex} relations in region III ($\lambda_{ex} > 340$ nm) for C28 and in regions II ($\lambda_{ex} = 310 \sim 370$ nm) and IV ($\lambda_{ex} > 420$ nm) for G28 are similar to the case of A28 and T28, although the fitting parameters (A, B) are obtained as (0.77, 160.2 nm), (0.34, 307.5 nm), and (1.75, −272.5 nm), respectively. These

FIG. 4. The diagram of the electronic energy levels and the corresponding transitions. Note that poorly stacked and well-stacked single bases coexist in ssDNA samples. Thus, the contributions of the stacked bases with exciton-state delocalization and the poorly stacked bases with coupled vibrational-electronic levels are dominated in the PL properties. For single base molecule, the electronic ground state, "dark" states (e.g., $^1n\pi^*$ states and triplets [9]), and excited singlet states are denoted by S_0, S_D, and S_1, respectively. For well-stacked bases, the electronic ground state, delocalized exciton states, and excimer state are labeled by S_0, S_{DE}, and S_E, respectively. For poorly stacked bases, the ground state and excited singlet state with coupled vibrational-electronic (vibronic) levels (fine solid lines in black and red) are denoted by S_0 and S_1, respectively. We use solid-line arrows to represent the electronic transitions with photon absorption or emission, whereas dotted-line arrows represent the transitions without the participation of photons. Meanwhile, IC, ISC, and VC are internal conversion, intersystem crossing, and vibrational cooling, respectively [40,41]. The nonradiative relaxation is denoted by NR.

PL behaviors are typical π-π^* transitions associated with coupled vibrational-electronic (vibronic) levels, as shown in the right panel of Fig. 4. By comparison with the single base molecule, the π electron delocalization in the ssDNA molecule with many repeat base units can reduce the energy of the excited singlet state S_1. Meanwhile, the atoms in a ssDNA molecule can vibrate about their bonds, which gives the molecule vibrational energy in addition its electronic energy (S_0 and S_1). Hence, a series of excited vibrational levels appear in S_0 and S_1, and the corresponding transitions show linear dependence between λ_{em} and λ_{ex}. This phenomenon is known as vibrational-electronic transitions, which can be understood by invoking the Frank-Condon principle [38]. This principle states that the nuclei do not move during the optical transitions, and is a consequence of the fact that electrons are much lighter than the nuclei. Therefore, the optical absorption and emission process does not alter the mean nuclear separation in the ground and excited states, but takes the molecule (electron) to the excited or ground state and changes the corresponding equilibrium nuclear separation. Then, a rapid nonradiative relaxation process, shown in the right panel of Fig. 4, can bring the molecule back to its equilibrium separation in the excited or ground state.

However, one may ask that why discrete and fine vibronic peaks are not observed in PL spectra shown by Fig. 2. Two reasons lead to the continuum spectra: (1) the ssDNA is a large molecule and possesses many vibrational modes of different frequencies, which produce overlapping progressions of vibronic lines that fill out into a continuum; (2) the thermal motion and collisions of the ssDNA and solvent molecules broaden the transitions so that the individual vibronic lines cannot be resolved. As a result, S_0 and S_1 for these regimes can be treated as quasi-energy-bands akin to the valence and conduction bands of a solid, as shown in the right panel of Fig. 4. In the bands of S_0 and S_1, we use n_{ex0} and n_{ex1} to label the vibronic levels associated with the absorption process, respectively, whereas we label the vibronic levels in the case of emission by using n_{em0} and n_{em1}, respectively. Based on the Franck-Condon principle, a common and simple model means that one can expect the emission spectrum to be the "mirror" of the absorption spectrum when reflected about the energy difference $\hbar\omega_0 \approx E_1 - E_2$, which means $n_{ex0} = n_{em1}$ (usually equals 0) and $n_{ex1} = n_{em0}$. This is known as the mirror symmetry rule [38]. Obviously, the mirror symmetry rule can result in decrease of λ_{em} with increasing λ_{ex}. Therefore, the roughly linear behavior of $\lambda_{em} = A\lambda_{ex} + B$ with $A > 0$ does not meet the mirror symmetry rule, which indicates

$n_{ex0} \neq n_{em1}$ or $n_{ex1} \neq n_{em0}$. For example, the excitation or absorption can be represented by $n_{ex0} = 0 \rightarrow n_{ex1} = 5$, but the emission process is $n_{em1} = 0 \rightarrow n_{em0} = 3 \neq n_{ex1}$, as shown in the part of $A > 0$ in Fig. 4. A possible reason for this phenomenon is that the nonradiative relaxation time increases almost linearly with lowering energy levels in the quasi-energy-bands [36]. Although the relaxation time cannot be obtained by nontransient PL experiment here, we can calculate the total energy shift induced by the nonradiative relaxation processes in the two quasibands through the following expression:

$$\Delta E_{\text{shift}} = hc\left(\frac{1}{\lambda_{ex}} - \frac{1}{A\lambda_{ex} + B}\right). \tag{1}$$

The ranges of ΔE_{shift} for different samples in the vibrational-electronic coupling domain obtained by using Eq. (1) are presented in Table II. Note that the separate energy shift in S_1 and S_0 cannot be distinguished in ΔE_{shift}, since the precise numbers of quanta for vibronic levels and the energy difference between adjacent levels are not known.

In regime II ($\lambda_{ex} = 310 \sim 330$ nm) for C28 and in regime III ($\lambda_{ex} = 380 \sim 410$ nm) for G28, we find that the λ_{em}-λ_{ex} relations are also roughly linear, but the emission peak wavelength shows a decrease or blueshift rather than increase behavior with increasing excitation wavelength. By fitting the experimental data with $\lambda_{em} = A\lambda_{ex} + B$, the parameters (A, B) can be obtained as $(-0.58, 606.8$ nm$)$ and $(-1.00, 810.5$ nm$)$ for C28 and G28, respectively. On one hand, from the perspective of phenomenological description, this blueshift behavior ($A < 0$) could also be explained in the same physical framework for the linear redshift behavior ($A > 0$) mentioned above. On the other hand, the λ_{em}-λ_{ex} relations with $A < 0$ can be understood by the mirror symmetry rule, which means $n_{ex0} = n_{em1}$ (usually equals 0) and $n_{ex1} = n_{em0}$ [38]. For example, the excitation process can be expressed as $n_{ex0} = 0 \rightarrow n_{ex1} = 2$, while the emission process is $n_{em1} = 0 = n_{ex0} \rightarrow n_{em0} = 2 = n_{ex1}$, as shown in the part of $A < 0$ in Fig. 4. One can deduce that the nonradiative relaxation time may decrease with lowering energy levels in the quasi-energy-bands of S_1 and S_0, which is contrary to the case of $A > 0$. Meanwhile, we can also calculate the ranges of ΔE_{shift} for different samples in these two regimes, as presented in Table II.

In an electronic system, the dependence of λ_{em} upon λ_{ex} should also rely on the electronic transition channels for photon emission. Therefore, we undertake the PL excitation (PLE) measurement on these ssDNA samples. PLE peaks correspond to the excitation wavelengths leading to high-efficiency emission with a fixed wavelength, which also can be treated as transition channels. The relative height of a PLE peak is usually proportional to the excitation efficiency. To some extent, the PLE spectrum can also reflect the electronic excitation and absorption channels of a material. Here the normalized PLE spectra are obtained by fixing an emission peak wavelength λ_{em} and scanning the excitation wavelength λ_{ex}. As shown in Fig. 5(a) to Fig. 5(d), since the PLE spectra for A- and T-base samples are similar, we first take the T-base ssDNA as the example for the investigation and analysis. The PLE spectra for T28, T35, and T56 are obtained at $\lambda_{em} = 419$ and 450 nm, which correspond to regime I ($S_E \rightarrow S_0$) and

regime II ($S_1 \rightarrow S_0$ with $A > 0$), respectively. As we can see, the normalized intensity of the PLE for the T-base sample enhances with the strand length (i.e., base number N), because T-base ssDNA with larger N possesses more electrons available for these transition behaviors associating with photon emission. Meanwhile, only one PLE peak can be observed at about $\lambda_{ex} = 345$ nm for $\lambda_{ex} = 419$ nm, corresponding to the dominated transition channel in the exciton-like transition behavior ($S_E \rightarrow S_0$). Although the channel is centered at $\lambda_{ex} = 345$ nm beyond regime I ($\lambda_{ex} = 300 \sim 330$ nm), its bandwidth covers this regime. The center wavelength only means that the 419 nm emission with highest efficiency can be obtained under excitations with $\lambda_{ex} = 345$ nm. Therefore, the exciton-like transition can occur for any excitation photons with λ_{ex} approaching the channel. In contrast, two peaks are obtained for $\lambda_{em} = 450$ nm at about $\lambda_{ex} = 345$ nm and 397 nm. They can be fitted via Gaussian functions (dashed curves), which indicate two transition channels associated with the PL emission of $S_1 \rightarrow S_0$ with $A > 0$. Accordingly, the competition between these two channels can be expected to result in the PL properties in this regime. However, to get the details of this process, time-resolved measurement may be necessary. This is beyond our discussion. Moreover, we also find that the excitation channel centered at 345 nm can contribute to the PL peaks corresponding to both regimes I and II. Interestingly, one can see from Fig. 5 that the PLE properties for A-base samples are similar to those for T-base samples, whereas the results of C- and G-base ssDNA show obvious differences.

By taking C-base ssDNA as an example, the PLE spectra measured at $\lambda_{em} = 430$ nm (regime I), 420 nm (regime II), and 450 nm (regime III) are illustrated in Figs. 5(e), 5(f), and 5(g), respectively. For comparison, the PLE spectra for C35 and C56 are also given besides C28. By examining the results for $\lambda_{em} = 430$ nm ($S_E \rightarrow S_0$) and 450 nm ($S_1 \rightarrow S_0$, $A > 0$), we can find two transition channels centered at $\lambda_{ex} = 345$ nm and 397 nm for most of the C-base samples, which are similar to those for the T-base samples in regime II. Furthermore, the PLE spectra measured for 420 nm ($S_1 \rightarrow S_0$, $A < 0$) also show a transition channel at 345 nm, but have a less obvious PLE peak at $\lambda_{ex} = 397$ nm. In addition, another channel can be observed near 306 nm for C28 and C35. This transition channel only slightly redshifts with increasing base number N, but disappears for a long strand such as $N = 56$. As mentioned above, the exciton state delocalization (in regime I) and the π electron delocalization (in regimes II to IV) in repeat base units can reduce the required photon energies for $S_0 \rightarrow S_{DE}$ and $S_0 \rightarrow S_1$ transitions. Therefore, a longer strand ssDNA possesses more repeat base units, which leads to a redshift of this absorption channel. However, if the strand is too long (e.g., $N = 56$), this channel is suppressed by the other two and the PLE peak near 306 nm disappears. For the case of G-base ssDNA in regimes I and III, we find two excitation channels at shorter (345 nm) and longer (384 nm) wavelengths, which is akin to the situation of C-base samples. Meanwhile, in the high-energy (UV) range, an excitation channel near 290 nm can be observed in Fig. 5(h) and Fig. 5(i), which could be compared with that near 306 nm for C-base ssDNA. However, for longer strand length, e.g., G35 and G56, the excitation efficiency of the transition channel centered at 384 nm shows
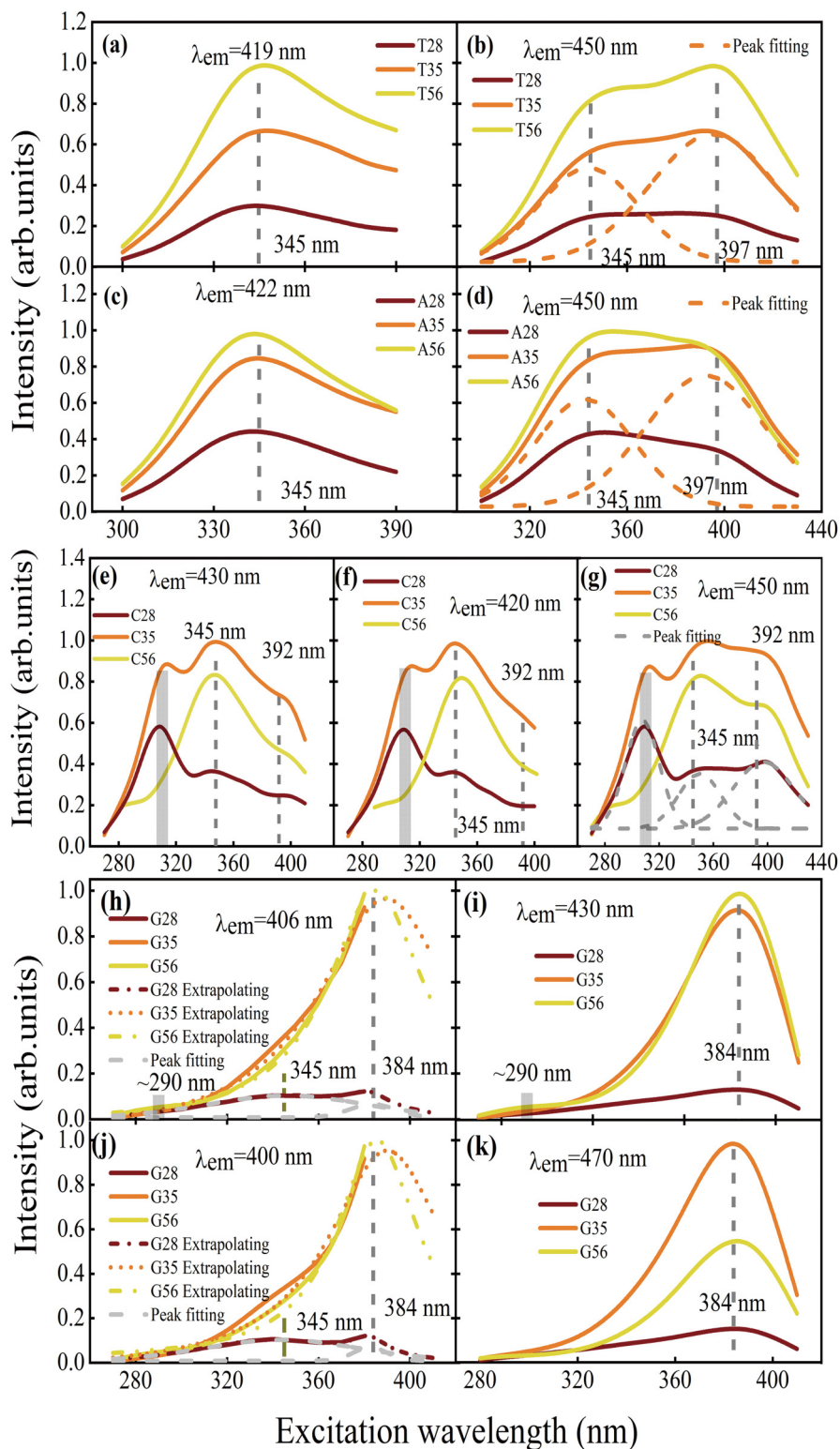
FIG. 5. Normalized PLE spectra measured at the fixed emission wavelengths corresponding to different regimes for T-, A-, C-, and G-base samples. The emission wavelengths are selected as (a) $\lambda_{em} = 419$ nm and (b) 450 nm for T-base samples, while those for A-base samples are fixed at (c) $\lambda_{em} = 422$ nm and (d) 450 nm. For C-base samples, (e) $\lambda_{em} = 430$ nm, (f) 420 nm, and (e) 450 nm are chosen to show the PLE spectra, whereas the situations of (h) $\lambda_{em} = 406$ nm, (i) 430 nm, (j) 400 nm, and (k) 470 nm are presented for G-base samples. Note that PLE peaks at 384 nm for G35 and G56 shown in (h) and (j) are obtained by extrapolating the measured data. The gray rectangles denote the ranges of the excitation channels in the high-energy (UV) regime. For C-base ssDNA, this channel is more sensitive to the strand length, whereas that for G-base sample is not obvious.

a remarkable increase. Thus, the spectral features (peaks) associating with the other two channels ($\sim$345 nm and $\sim$290 nm) are suppressed in different degree. This fact hampers our further investigation into their behaviors. Accordingly, other kinds of experimental research, such as transient PL and absorption spectroscopy, can be expected to clarify these processes, which are beyond the main topic of this work.

Based on the analysis for the PL and PLE spectra of ssDNA, we establish a general description for the electronic states and transition behaviors of A-, T-, C-, and G-based ssDNA samples under NUV and visible excitations. Our theoretical framework can not only explain the phenomena observed here, but also supports some relevant experimental results reported in previous works [24,26,27,39]. It should be noted that in addition to some traditional concepts associated with electronic transitions borrowed from solid-state physics, the framework obtained here is also based on the theory of vibrational-electronic (vibronic) transitions. Therefore, the model of molecular vibrational levels without vibrational-electronic coupling is not suitable for the explanation to our experimental results. The reasons are listed as follows: (1) It is well known that the vibrational resonances (vibrational levels) of most biological molecules are located in the infrared and terahertz regimes instead of the NUV and visible regimes. For example, mid-IR pulses can probe vibrational transition dynamics of single-base excited states of DNA via bleach recovery of ground-state fundamentals ($1625\ \mathrm{cm}^{-1}$) as well as hot band decay (1590–$1615\ \mathrm{cm}^{-1}$) [9]. (2) As shown in Fig. 4, the vibrational cooling process is also included for a single base. For a single base and poorly stacked bases, vibrational cooling returns the molecule to thermal equilibrium with the solvent, which is a nonradiative relaxation process [9,26].

Moreover, the measurements of fluorescence anisotropy would be helpful to improve the physical discussion proposed here. However, two reasons limit our further study on this property. First, Callis demonstrated that the PL polarization (fluorescence anisotropy) at room temperature for most of the DNA bases is considerably less than at low temperature (e.g., $-125\,^{\circ}\mathrm{C}$) [17]. It is obvious that the DNA solutions at room temperature are liquid. Therefore, the orientation of the DNA molecules is highly random, which leads to low PL polarization. In addition, the concentrations of our ssDNA samples are about 100 to 1000 times lower than those of the DNA samples used in Ref. [17]. Thus, the performance of polarization-resolved PL measurements will be much poorer. Based on these points, we encourage future works to focus on the fluorescence anisotropy of ssDNA excited by NUV and visible light for high-concentration samples or at low temperatures or in a solution with weak absorption of the excitation and emission light beams.

IV. CONCLUSIONS

In summary, by using nontransient PL and PLE measurements under NUV and visible excitations, the PL properties of A-, T-, C-, and G-based ssDNA samples with different strand lengths are investigated. The PL behaviors of all the samples can be roughly classified into two categories according to the λ_{em}-λ_{ex} relations and physical mechanisms. One can be ascribed to exciton-like transitions associated with delocalized exciton states and excimer states. Thus, the PL peak position of ssDNA is nearly constant in a relatively short excitation wavelength regime. The other comes from electronic transitions related to quasi-energy-bands composed of coupled vibrational-electronic levels, which shows a linear relation of $\lambda_{\mathrm{em}} = A\lambda_{\mathrm{ex}} + B$ with $A > 0$ or $A < 0$ in relatively long excitation wavelength range. Meanwhile, we also obtain the transition channels for different excitation wavelength regimes and analyze the effects of strand length and base type. These results are not only essential for understanding the electronic structure of DNA excited by NUV and visible light, but also important for the nanoelectronic or optoelectronic applications realized by DNA.

[1] J. D. Watson and F. H. C. Crick, Nature (London) **171**, 737 (1953).

[2] K. H. Yoo, D. H. Ha, J. O. Lee, J. W. Park, J. Kim, J. J. Kim, H. Y. Lee, T. Kawai, and H. Y. Choi, Phys. Rev. Lett. **87**, 198102 (2001).

[3] E. Braun, Y. Eichen, U. Sivan, and G. B. Yoseph, Nature (London) **391**, 775 (1998).

[4] A. Rakitin, P. Aich, C. Papadopoulos, Yu. Kobzar, A. S. Vedeneev, J. S. Lee, and J. M. Xu, Phys. Rev. Lett. **86**, 3670 (2001).

[5] H. Yan, S. H. Park, G. Finkelstein, J. H. Reif, and T. H. Labean, Science **301**, 1882 (2003).

[6] I. Willner, B. Shlyahovsky, M. Zayats, and B. Willner, Chem. Soc. Rev. **37**, 1153 (2008).

[7] C. E. Crespo-Hernández, B. Cohen, and B. Kohler, Nature (London) **436**, 1141 (2005).

[8] S. Marguet and D. Markovitsi, J. Am. Chem. Soc. **127**, 5780 (2005).

[9] C. T. Middleton, K. de La Harpe, C. Su, Y. K. Law, C. E. Crespo-Hernández, and B. Kohler, Annu. Rev. Phys. Chem. **60**, 217 (2009).

[10] P. Carpena, P. Bernaola-Galvan, P. C. Ivanov, and H. E. Stanley, Nature (London) **418**, 955 (2002).

[11] R. G. Endres, D. L. Cox, and R. R. P. Singh, Rev. Mod. Phys. **76**, 195 (2004).

[12] D. Voet, W. B. Gratzer, R. A. Cox, and P. Doty, Biopolymers **1**, 193 (1963).

[13] A. GraSlund, H. Steen, and A. Rupprecht, Int. J. Radiat. Biol. **30**, 263 (1976).

[14] K. R. Koswattage, Y. Izumi, and K. Nakagawa, Quantum Beam Sci. **4**, 30 (2020).

[15] H. Qu, C. Hao, Z. Nan, X. Zhang, and R. Sun, Spectrochim. Acta, Part A **224**, 117459 (2020).

[16] S. Basu, R. B. Cundall, and M. W. Jones, Chem. Phys. Lett. **53**, 439 (1978).

[17] P. R. Callis, Chem. Phys. Lett. **61**, 568 (1979).

[18] J. Peon and A. H. Zewail, Chem. Phys. Lett. **348**, 255 (2001).

[19] K. de La Harpe and B. Kohler, in *International Conference on Ultrafast Phenomena 2010, Snowmass, Colorado, 18–23 July 2010* (The Optical Society, 2010)

[20] J. Chen, Y. Zhang, and B. Kohler, Top. Curr. Chem. **356**, 39 (2014).

[21] C. E. Crespo-Hernández, B. Cohen, P. M. Hare, and B. Kohler, Chem. Rev. **104**, 1977 (2004).

[22] J. Eisinger and A. A. Lamola, *The Excited States of Nucleic* (Springer US, 1971).

[23] P. R. Callis, Annu. Rev. Phys. Chem. **34**, 329 (1983).

[24] J. W. Longworth, R. O. Rahn, and R. G. Shulman, J. Chem. Phys. **45**, 2930 (1966).

[25] A. Anders, Chem. Phys. Lett. **81**, 270 (1981).

[26] I. Buchvarov, Q. Wang, M. Raytchev, A. Trifonov, and T. Fiebig, Proc. Natl. Acad. Sci. USA **104**, 4794 (2007).

[27] B. Dong, L. M. Almassalha, Y. Stypula-Cyrus, B. E. Urban, J. E. Chandler, T. Nguyen, C. Sun, H. F. Zhang, and V. Backman, Proc. Natl. Acad. Sci. USA **113**, 9716 (2016).

[28] K. Hyeon-Deuk, Y. Tanimura, and M. Cho, J. Chem. Phys. **128**, 135102 (2008).

[29] E. B. Starikov, G. Cuniberti, and S. Tanaka, J. Phys. Chem. B **113**, 10428 (2009).

[30] I. Kalnina, R. Bruvere, T. Zvagule, N. Gabruseva, L. Klimkane, E. Kirilova, I. Meirovics, and G. Kizane, J. Fluoresc. **20**, 9 (2010).

[31] G. Paës, Molecules **19**, 9380 (2014).

[32] C. Ma, W. Sun, L. Xu, Y. Qian, J. Dai, G. Zhong, Y. Hou, J. Liu, and B. Shen, J. Mater. Chem. B **8**, 9642 (2020).

[33] P. Sun, H. Zhang, Y. Sun, and J. Liu, Spectrochim. Acta, Part A **245**, 118919 (2020).

[34] L. J. Mcbride and M. H. Caruthers, Tetrahedron Lett. **24**, 245 (1983).

[35] H. M. Buck, Nucleosides, Nucleotides Nucleic Acids **34**, 400 (2015).

[36] C. J. Li, L. Ding, C. N. Liang, J. Zhang, C. Zhang, H. Y. Mei, C. Wang, W. D. Wu, J. Zhang, and W. Xu, ACS Omega **2**, 5759 (2017).

[37] J. Zhang, L. Ding, S. Zhou, Y. M. Xiao, and W. Xu, Phys. Status Solidi RRL **14**, 2000222 (2020).

[38] M. Fox, *Optical Properties of Solids* (Oxford University Press, New York, 2001).

[39] J. Eisinger, M. Guaron, R. G. Shulman, and T. Yamane, Proc. Natl. Acad. Sci. USA **55**, 1015 (1966).

[40] H. Kang, B. Jung, and S. K. Kim, J. Chem. Phys. **118**, 6717 (2003).

[41] T. Fuji, H. J. Ong, and T. Kobayashi, Chem. Phys. Lett. **380**, 135 (2003).